Terahertz Vibrational Modes of Sodium Magnesium Chlorophyllin and Chlorophyll in Plant Leaves

Dominique Coquillat*[1], Emma O'Connor[2], Etienne V. Brouillet*[3], Yoann Meriguet[1,4], Cédric Bray[1], David J. Nelson[3], Karen Faulds[2], Jeremie Torres[4], Nina Dyakonova[1]

[1]Laboratoire Charles Coulomb (L2C), Université de Montpellier, CNRS, Montpellier, France.
[2]Centre for Molecular Nanometrology, WestCHEM, Department of Pure and Applied Chemistry, Technology and Innovation Centre, University of Strathclyde, 99 George Street, Glasgow, G1 1RD, Scotland.
[3]WestCHEM Department of Pure and Applied Chemistry, University of Strathclyde, 295 Cathedral Street, Glasgow, G1 1XL, Scotland.
[4]Institut d'Electronique et des Systèmes (IES), Université de Montpellier, CNRS, Montpellier, France.

*Corresponding authors: dominique.coquillat@umontpellier.fr, etienne.brouillet@gmail.com

Abstract
The low-frequency (terahertz) vibrational spectroscopy has been investigated experimentally for two chlorophyll species, Chl-a and one of its magnesium derivatives (Chl-Mg-Na). The combination of terahertz time-domain spectroscopy and Fourier transform infrared spectroscopy has enabled a broad frequency range to be covered (0.2 to 18 THz). For Chl-Mg-Na, the terahertz spectra show clear and well-marked features at 1.44, 1.64, and 1.83 THz dominated by intermolecular interactions. The frequency dependent refractive index and absorption coefficient of Chl-Mg-Na were both determined using the Fit@TDS software. Below 1.0 THz, a refractive index of 2.09 was measured. In order to acquire further understanding of the observed vibrational modes, a detailed study of the temperature dependence of the line positions of the lowest modes in Chl-Mg-Na was performed. As the temperature was increased from 88 K to 298 K, the feature at 1.83 THz experienced a notable red shift of frequency and line shape broadening, whereas the feature at 1.44 THz showed little change. These results suggest that the 1.83 THz feature is dominated by intermolecular motions occurring over the crystalline unit cell of the Chl-Mg-Na molecular crystal. Finally, terahertz time-domain spectroscopy was used to acquire the spectra of an ornamental plant bearing yellow-green variegated leaves (ivy, *Aureomarginata* variety), the yellow sectors having lower chlorophyll content compared to the green sectors. In dehydrated green tissue, the chlorophyll molecules showed well-marked intermolecular vibrational modes at 1.86 THz, indicating that chlorophyll molecules are prone to packing with an ordered molecular arrangement. These results demonstrate the potential application of THz spectroscopy in the field of agronomy.

Keywords Terahertz spectroscopy, chlorophyll derivatives, chemical recognition, bio-sensing, plant leaf, life sciences,

1 Introduction

Chlorophyll is a group of important photosynthetic pigments in plants, playing an essential role in light harvesting and conversion processes. Chlorophyll and its semisynthetic derivatives have long found wide application as food colorants and therapeutic agents. In addition, the focus on chlorophyll derivatives has recently been boosted by their application as efficient catalysts [1], functional materials in molecular electronics [2-4] and as photoactive materials for new types of solid-state biosolar cells [5,6]. The properties making chlorophyll and their derivatives so versatile arise from their chemical structures which influence their absorption and emission spectra. Therefore, it is expected that all aspects of their spectra in the ultraviolet-visible, infrared, and far-infrared regions have been thoroughly studied by spectroscopic techniques. Although some papers have reported the study of the vibrational modes of natural chlorophylls and chlorophyll derivatives using Fourier transform infrared (FTIR) spectroscopy [7-9] and Raman spectroscopy [10,11], they have merely presented intramolecular vibrational properties of the molecules for frequency ranges above 5 THz (167 cm^{-1}). Thus, the THz spectroscopy (with frequencies between 100 GHz and 10 THz) which is sensitive to low frequency intermolecular and intramolecular vibrational modes in molecular crystals [12-20] remains to be explored. Other techniques such as single crystal X-ray diffraction (XRD) can be used to elucidate the crystal structure of molecular crystals. However, this technique requires a suitable crystalline material, which is often difficult to obtain in the case of chlorophyll and its close derivatives [21]. XRD

This is a peer reviewed, accepted author manuscript of the following research article: Coquillat, D., O'Connor, E., Brouillet, E. V., Meriguet, Y., Bray, C., Nelson, D. J., Faulds, K., Torres, J., & Dyakonova, N. (Accepted/In press - 13 January 2023). Terahertz vibrational modes of sodium magnesium chlorophyllin and chlorophyll in plant leaves. *Journal of Infrared, Millimeter and Terahertz Waves*.

provides a static three-dimensional structure that may not account for the lattice dynamics occurring in the crystal, which can provide additional valuable structural information. THz time-domain spectroscopy (THz-TDS) detects low frequency vibrational modes directly linked to the packing structure and to the long-range forces from neighbouring molecules, making it a powerful technique to gain structural information of polycrystalline powder of chlorophyll pigments [12-20]. Furthermore, the application of THz-TDS to pigment molecules found in plants has been limited [22-25], and there is scope to better understand their properties in this part of the spectrum. The extension of such investigations to chlorophyll in plant tissues would offer a rich but challenging sector of study. Investigating the low-frequency vibrations of chlorophyll derivatives will be helpful for not only completing the data library of the THz properties of materials, but also for a better understanding of the THz properties of the natural chlorophylls, chlorophyll derivatives, and of more complex structures related to chlorophyll [26].

Chlorophyll is a group of fat-soluble magnesium porphyrin complexes, *e.g.* Chl-a, which are predominantly found in green sectors of plants. Sodium magnesium chlorophyllin (Chl-Mg-Na) is a semisynthetic derivative of chlorophyll which displays additional advantageous properties, including good water solubility, excellent photosensitivity, and thermal- and photo-stability. The molecular structures Chl-a and Chl-Mg-Na are shown in Fig. 1. The structure of Chl-a consists of a porphyrin ring, whose four nitrogen atoms surround a central magnesium atom, with several other functional groups (e.g. ester, ketone) and a hydrocarbon tail (Fig. 1a). The structure of Chl-Mg-Na has a similar asymmetric porphyrin ring but lacks the long flexible hydrocarbon chain (Fig. 1b). Chl-Mg-Na is thus more stable to long-term irradiation and exhibits characteristic blue and red absorption bands that are very close to those of Chl-a. Comparing the spectroscopic properties of both compounds by THz techniques will strengthen the library of the THz properties of materials and identify differences and similarities between natural chlorophyll and its semisynthetic derivatives.

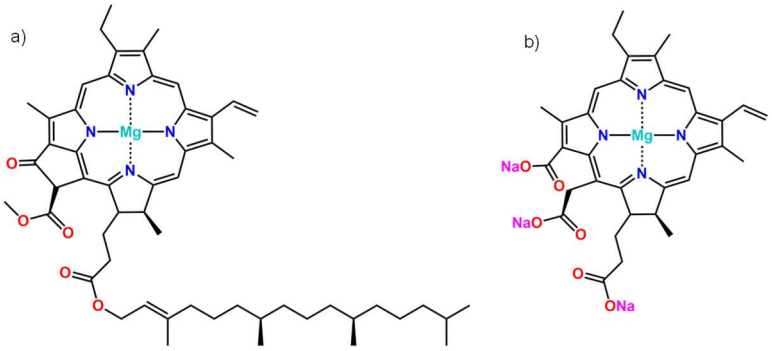

Fig. 1 Molecular structure of a) natural chlorophyll, Chl-a, and b) semisynthetic sodium magnesium chlorophyllin (Chl-Mg-Na).

Here, using THz spectroscopy, we offer an alternative to previously proposed spectroscopic techniques *i.e.* ultraviolet-visible and infrared. This study is focused on Chl-a and its derivative Chl-Mg-Na. Firstly, FTIR and surface-enhanced Raman scattering (SERS) were used to obtain complementary information about the intramolecular interactions for both of these species. THz-TDS was then used to identify the distinct spectral fingerprints corresponding to the low-frequency vibrational modes in the region that includes intermolecular interactions. The spectral signature of Chl-Mg-Na was also investigated as a function of temperature. Following the identification of these distinct fingerprints, our study focused on the direct detection of chlorophyll in plant tissues. Only a few studies attempted to discover Chl-a fingerprint in plant leaves at THz frequencies [24-27]. Through the identification of the spectral fingerprint of Chl-a, we can use this newly gained knowledge to demonstrate that the identification of chlorophyll was possible in dehydrated plant tissues. This is a first step in the observation of chlorophyll in plants using this new approach, the understanding of which could which could prove invaluable to the field of plant physiology and agronomy.

2 Experimental

2.1 Chl-a and chlorophyll derivative samples preparation

Chl-*a* powder purchased from Sigma-Aldrich was stored in the dark at -25°C before preparing pellets. Chl-Mg-Na powder was purchased from Catalyons and according to the manufacturer, 0.5% magnesium stearate was added as a lubricant. Nevertheless, the powder was used without any further purification. The chlorophyll derivative samples used for mass spectroscopy, absorption spectra in the visible range and for surface-enhanced Raman scattering (SERS) were dispersed in water or methanol at appropriate mass ratios. For SERS measurements, colloidal silver nanoparticles (AgNPs) were added to the solutions. The samples used for THz-TDS and FTIR measurements were prepared by mixing the polycrystalline Chl-*a* or Chl-Mg-Na and high-density polyethylene (PE) powders. The mixtures were then pressed with an applied pressure of 5 tons for three minutes. The resulting pellets have a diameter of 13 mm. The Chl-*a*-PE pellet has a small amount of chlorophyll: less than 5 mg in 100 mg PE. In contrast, having a large amount of Chl-Mg-Na powder, a fairly large number of Chl-Mg-Na-PE pellets were prepared, with different concentrations and thicknesses. These pellets, necessary for measuring the THz transmission in a suitable frequency range, contained from 10 to 50 weight-percent (wt-%) of Chl-Mg-Na within the PE matrix and have thicknesses between 50 µm and 1.2 mm. Moreover, as the chlorophyll derivative powders compact well, pellets containing only Chl-Mg-Na were prepared. Pellets containing from 0.5 to 2.0 wt-% of magnesium stearate within the PE matrix were also prepared. Table 1 summarizes the different pellet fabrication conditions.

Table 1 Weight of pellets containing different relative amounts of PE and Chl-*a*, of PE and Chl-Mg-Na, of PE and magnesium stearate, and of PE and dehydrated ivy tissues. The mixture composition is given in weight-percent (wt-%).

Pellet No.	Mixture composition	Pellet Mass (mg)	Substance Quantity (mg)	Measurements
1	~ 4.0 wt-% Chl-*a*	115.0	4.6	FTIR &THz-TDS at 298 K
2	100 wt-% Chl-Mg-Na	202.8	202.8	THz-TDS at 298 K
3	100 wt-% Chl-Mg-Na	179.6	179.6	THz-TDS at 298 K
4	100 wt-% Chl-Mg-Na	97.9	97.9	THz-TDS at 298 K
5	100 wt-% Chl-Mg-Na	72.6	72.6	THz-TDS at 298 K
6	100 wt-% Chl-Mg-Na	77.8	77.8	THz-TDS at 298 K
7	100 wt-% Chl-Mg-Na	60.0	60.0	THz-TDS vs temperature
8	50.0. wt-% Chl-Mg-Na	302.6	151.3	THz-TDS at 298 K
9	50.0 wt-% Chl-Mg-Na	202.0	101.0	THz-TDS at 298 K
10	50.0 wt-% Chl-Mg-Na	60.1	30.0	THz-TDS at 298 K
11	30.0 wt-% Chl-Mg-Na	116.8	35.0	THz-TDS at 298 K
12	30.0 wt-% Chl-Mg-Na	83.2	25.0	THz-TDS at 298 K
13	42.5 wt-% Chl-Mg-Na	72.6	30.9	FTIR at 298 K
14	25.7 wt-% Chl-Mg-Na	61.0	15.7	FTIR at 298 K
15	25.7 wt-% Chl-Mg-Na	37.3	9.6	FTIR at 298 K
16	17.2 wt-% Chl-Mg-Na	79.2	13.6	FTIR at 298 K
17	100 wt-% PE	116.8	116.8	THz-TDS at 298 K
18	100 wt-% PE	98.7	98.7	THz-TDS at 298 K
19	0.5 wt-% magnesium stearate	300.0	1.5	THz-TDS at 298 K
20	2.0 wt-% magnesium stearate	300.0	6.0	THz-TDS at 298 K
20	50.0 wt-% dehydrated ivy green tissue	200.0	100.0	THz-TDS at 298 K & 88 K
21	50.0 wt-% dehydrated ivy yellow tissue	185.0	92.5	THz-TDS at 298 K & 88 K

2.2 Plant Material

To investigate the intermolecular vibrational properties of chlorophyll molecules in plant tissues, well developed leaves of the variegated ivy were examined (*Aureomarginata* variety). For the *Aureomarginata* variety, leaves show a green centre, a yellow margin and intermediate pale green sectors. For THz-TDS transmission experiments, the yellow and green sectors of mature and fresh leaves were separated by cutting and used to prepare yellow or green powders. The powders were both mixed with PE and compressed into 13 mm diameter pellets by applying a constant pressure of 5 tons for three minutes.

2.3 Mass Spectroscopy

Electrospray ionization mass spectroscopy analysis (ESI-MS) and MS/MS experiments were performed on the Chl-Mg-Na product, the mass spectrometer operating in the positive mode. The MS-spectra were acquired by full

range covering the scale m/z 100-1000. For the fragmentation study, MS/MS experiments were performed by deploying collision-induced dissociation with the normalized collision energy set between 10 and 50 eV.

2.4 Surface-Enhanced Raman spectroscopy

Complementary information about intramolecular vibrations of Chl-Mg-Na was investigated by SERS detection. For SERS spectra acquisition, the excitation photon wavelength (532 nm) was close in wavelength to the Q_y band [28] (see the Supporting Information), the spectral window recorded was between 200 and 1600 cm^{-1}, and each SERS spectrum was an average of 3 successive scans. Chl-Mg-Na was found to be readily soluble in water, but only slightly soluble in methanol. As a result, the absorption of Chl-Mg-Na recorded by a UV-Vis-NIR spectrometer showed that the Q_y band shifted slightly from 653 nm for the aqueous solution (1 mg/mL solution diluted to 60 µg/mL in H_2O) to 648 nm for the methanol suspension (0.5 mg/mL in MeOH further diluted to 25 µg/mL in MeOH)) (Supporting Information). In the SERS study, three solutions were analysed. Solution 1 (S1) was prepared by adding 1 mL of MeOH to 0.54 mg of Chl-Mg-Na. Solution 2 (S2) was prepared by mixing 200 µL of AgNPs (40 nm citrate-capped AgNPs at 0.03 nM) with 200 µL of S1. Solution 3 (S3) was prepared by adding 100 µL a 0.1 M aqueous solution of NaCl to S2. Addition of NaCl to AgNPs promotes aggregation of the nanoparticles, a key role to the signal enhancements observed in SERS. The laser power (incident laser power was 40 mW) was set at 2 mW for S1 and S2, 4 mW for S3 and an average scan time of 0.5 s was used for all solutions.

2.5 Terahertz spectroscopy

Low-frequency vibrational modes of Chl-a and Chl-Mg-Na were collected in transmission configuration with THz-TDS and FTIR spectrometers, to cover the spectral absorption range from 0.2 THz to 18 THz.

FTIR Spectroscopy experimental setup. FTIR spectroscopy is most useful in high frequency range of the THz spectra and has low signal/noise ratio at lower frequencies. Measurements were performed with a Brucker IFS 66v/S spectrometer that accesses the THz range using a liquid helium cooled bolometer. The transmission was measured in vacuum over the frequency range (0.5-18 THz) with a spectral resolution of 0.5 cm^{-1} (0.015 THz). FTIR spectra were acquired with at least 100 scans. The FTIR spectra were normalized using the empty aperture as a reference. The absorbance spectra were calculated and had a background correction using the Vancouver algorithm [29] with a 5^{th} order polynomial fit (Supporting Information). FTIR spectroscopy can obtain amplitude information only.

THz-TDS experimental setup. THz-TDS has the advantage of simultaneously obtaining amplitude and phase of coherently generated THz radiation, and providing a better signal to noise ratio than FTIR spectroscopy at frequencies below 3 THz (100 cm^{-1}). THz-TDS and FTIR can thus complement each other for the study of intramolecular and intermolecular vibrational modes. The THz-TDS spectra were acquired using a commercial TeraPulse 4000 instrument (TeraView Ltd, Cambridge, UK) across the spectral range of 0.1-3.5 THz. To minimize the contribution of the water vapour to the sample spectrum, the sample chamber was either purged continuously with dry nitrogen or evacuated throughout the measurements. For a given sample, the empty aperture was used as a reference and the raw absorbance calculated. In addition, the peaks associated to the low-frequency vibrational modes were treated as the spectra of interest. Then, to eliminate the varying background mainly caused by the presence of amorphous, disordered regions in the samples, the raw absorbance calculation was followed by a background correction using the Vancouver algorithm with a 5^{th} order polynomial fit [29]. Variable temperature experiments were performed using a liquid nitrogen cooled cryostat. The spectra were acquired while cooling over a temperature range, from 298 to 88 K. At each temperature, the samples were left to equilibrate for approximately 10 min before starting measurements.

3 Results and discussion

3.1 FTIR and SERS spectra

Our initial efforts to explore low-frequency vibrational modes of chlorophyll have focused on polycrystalline Chl-a, for which intramolecular vibrations at frequencies above 5 THz (167 cm^{-1}) have already been explored with solutions, suspensions [8] and solid films [9]. Our measured far-infrared absorbance spectra of the Chl-a-PE pellet containing a low amount of Chl- a (pellet 1, around 4.0 wt-%) are presented in Fig. 2a, after normalization and background correction with the Vancouver algorithm. The results from the FTIR experiments plotted between 4.5

and 11 THz (150 and 367 cm^{-1}) show that the main far-infrared spectral features of Chl-*a* molecules have three strong characteristic absorption bands centred at 6.01 THz (200 cm^{-1}), 8.83 THz (295 cm^{-1}), and 9.24 THz (308 cm^{-1}). These peak positions, reported in Table 2, agree well with the spectra presented in Refs. 8 and 9. Far-infrared studies have shown that aggregation of chlorophyll induces a supplementary 300-312 cm^{-1} absorption band. The features above 200 cm^{-1} primarily correspond to intramolecular bonds in Chl-*a*. Many of the features have been assigned [7-9] and relate mainly to skeletal deformations of the porphyrin section of the Chl-*a* molecule, with strong contributions from Mg-N or Mg-O bending and stretching modes. A similar analysis may be applied to the far-infrared and THz spectra of Chl-Mg-Na but to our knowledge, there are no results available in the literature. Far-infrared absorbance spectra were obtained using different concentrations of Chl-Mg-Na powder in the PE matrix (pellets 13 to 16, Table 1) and are reported in Fig. 2b. Compared to the far-infrared spectra of Chl-*a* in Fig. 2a, a number of well-resolved and narrower absorption peaks are seen in the range 3-18 THz (100 – 600 cm^{-1}).

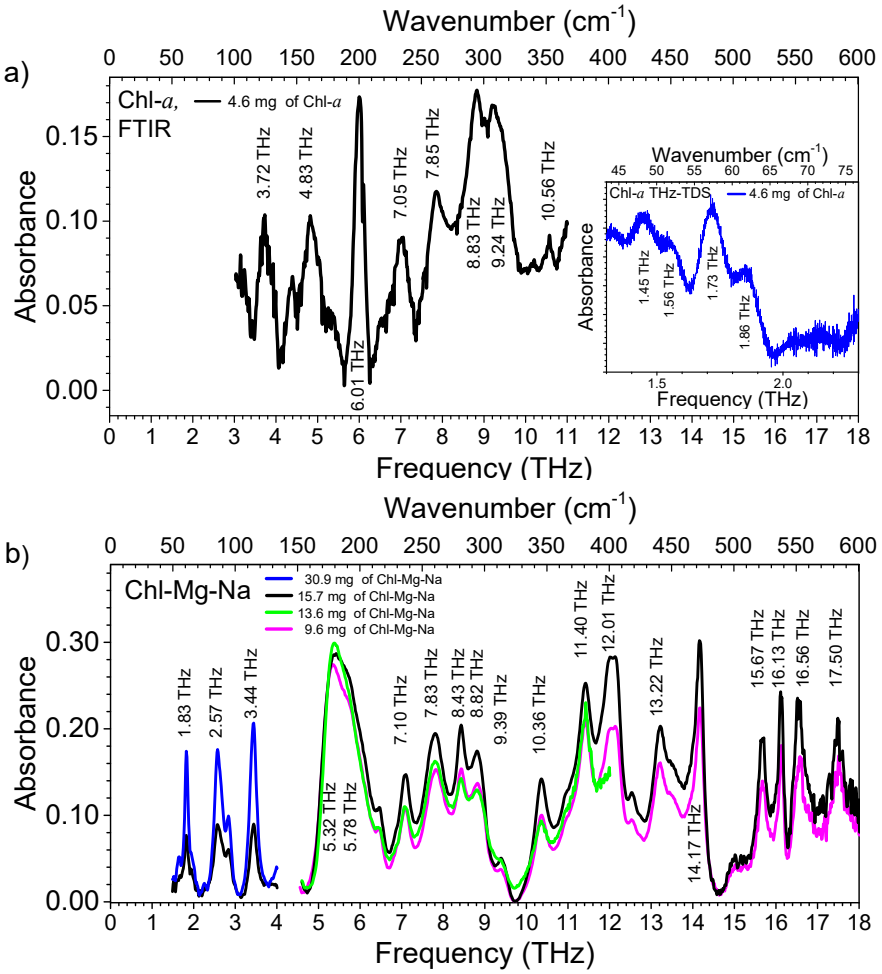

Fig. 2 Background corrected absorbance spectra measured by FTIR at room temperature of a) Chl-*a* (pellet 1, black), and b) Chl-Mg-Na, for different mixtures of Chl-Mg-Na and PE powders (pellet 13, blue; pellet 14, black; pellet 15, pink; pellet 16, green). Inset of Fig. 2a: THz-TDS spectrum of Chl-*a* (pellet 1, blue).

The higher Chl-Mg-Na concentration (pellet 13, blue curve) led to saturation of the strong absorption band centred at 5.32 THz (177 cm^{-1}) in the far-infrared spectrum but resulted in more pronounced peaks in the THz range (Fig. 2b). These peaks will be discussed in more detail in the Section 3.2. In addition to the major peaks reported in Table 2, many weaker features appeared, which leads to peak broadening, and formation of shoulders. Complementary SERS experiments were also carried out. While the intensity of many bands typically changes in both SERS and FTIR spectra, SERS combines the specificity of vibrational Raman spectroscopy with the increased sensitivity provided by plasmon assisted scattering, induced by the presence of colloidal AgNPs [30]. Further enhancement of the SERS signal can be gained by adding salt to colloidal AgNPs, this causes slight aggregation

of the nanoparticles and leads to the formation of SERS 'hotspots' [31]. Figure 3 presents Raman spectrum of Chl-Mg-Na in solution and SERS spectra in presence of AgNPs. The peaks in this frequency range (200-1600 cm^{-1}) are governed by the intramolecular vibrations of the sample. Below 400 cm^{-1}, the Chl-Mg-Na solution exhibits a broad feature in the 290-310 cm^{-1} region (8-69-9.29THz) observed in FTIR spectra and arising from aggregation. The comparison of the SERS absorption peaks of Chl-Mg-Na with both SERS [10] and resonant Raman spectra of Chl-a [11] reveals that the SERS spectrum of Chl-Mg-Na is almost similar to that of Chl-a. Most of the frequency difference are less than 10 cm^{-1}. In the intramolecular frequency range, the SERS spectra of the natural Chl-a and of Chl-Mg-Na being qualitatively similar suggests that the features observed at 302 and 340 cm^{-1} in the Chl-Mg-Na spectrum can be assigned to MgN_4 intramolecular vibrations.

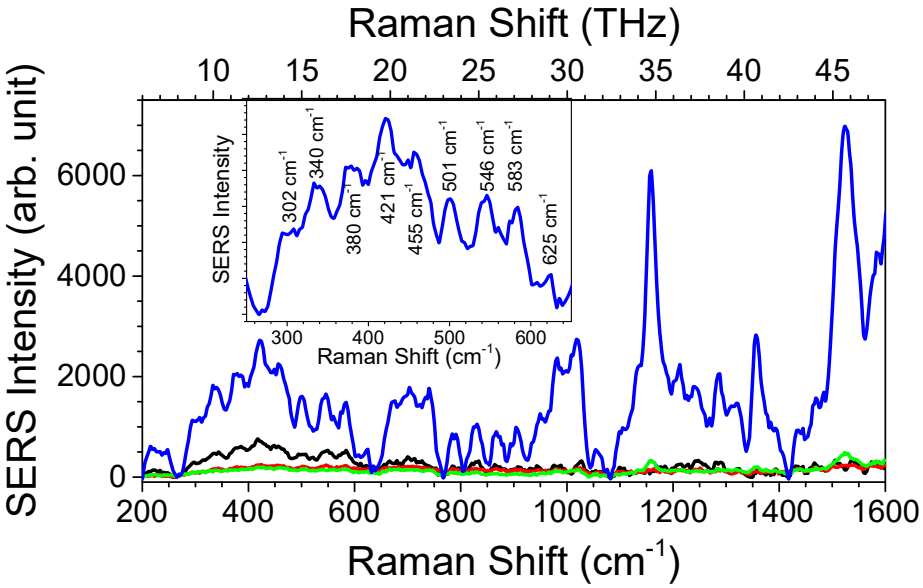

Fig. 3 Background corrected Raman spectrum of Chl-Mg-Na in solution and SERS spectra in presence of AgNPs for two solutions. Black curve: S1: Chl-Mg-Na in MeOH (0.54 mg/mL), 5% laser power; red curve: S2: S1 + 200 µL AgNPs, 5% laser power (2 mW); green curve: S3: S2 + 100 µL 0.1 M NaCl, 5% laser power; (2 mW) blue curve: S3: S2 + 100 µL 0.1 M NaCl, 10% laser power (4 mW). Inset: Enlarged view of the 250-650 cm^{-1} region.

Table 2 Frequency position of THz and far-infrared absorption features of Chl-*a* and of Chl-Mg-Na at room temperature (in THz and in cm^{-1}). Data from other reports are also included*,♦,♠,♣,♥.

Chl-*a*					Chl-Mg-Na		
Chl-*a* THz-TDS & FTIR (This work)	Chl-*a*♦ THz-TDS	Chl-*a*♠ THz-TDS	Chl-*a*♣ FTIR	Chl-*a*♥ FTIR	Chl-Mg-Na THz-TDS (This work)	Chl-Mg-Na FTIR (This work)	Chl-Mg-Na SERS (This work)
1.45 (48.4) s		1.42 (47.4) s			1.442 (48.1) s		
1.56 (52.0) w	1.64 (54.7) s				1.535 (51.2) vw		
1.73 (57.7) vs	1.72 (57.4) vs	1.68 (56.0) sb			1.637 (54.6) m		
1.86 (62.0) s	1.86 (62.0) vs				1.823 (61.3) vs	1.83 (60.8) vs	
	1.98 (66.0) s				1.96 (65.4) m		
		2.45 (81.7) m			2.03 (67.7) vw		
3.72 (124) m					2.24 (74.6) w	2.24 (74.6) w	
4.83 (161) m			5.46 (182) w	5.70 (190) mb	2.57 (85.8) m	2.57 (85.8) s	
6.01 (200) vs			5.97 (199) mb	6.24 (208) sb	2.84 (94.5) m	2.84 (94.5) m	
7.05 (235) m				6.48 (216) m		3.44 (114) s	
7.85 (262) m			7.85 (262) w	7.31 (244) w		5.32 (177) vsb	
8.83 (295) vs				8.24 (275) m		5.78 (193) vsb	
9.24 (308) vs			9.08 (303) vs	9.11 (304) mb		6.47 (216) w	
10.56 (352) m			10.40 (347) m			7.10 (237) m	
			11.39 (380) w	11.33 (378) vs		7.83 (261) s	
			11.93 (398) s			8.43 (281) vs	
				13.01 (434) s		8.82 (294) vs	8.69-9.29
			13.97 (466) m	13.76 (459) m		9.39 (313) m	(290-310) m
			14.27 (476) w			10.36 (345) m	10.19 (340) m
						10.96 (365) s	10.85 (362) m
						12.01 (400) s	11.09-11.69
							(370-390) mb
						12.14 (405) s	
						12.54 (418) w	12.62 (421) s
						13.22 (441) m	13.64 (455) m
						14.17 (472) vs	14.24 (475) w
						15.02 (501) wb	15.02 (501) m
						15.67 (522) s	
						16.13 (538) s	
						16.56 (552) s	16.37 (546) m
						17.50 (583) m	17.50 (583) m

*Entries: s, strong; m, medium; w, weak; b, broad; v, very. ♦ Data from Wagner [24], ♠ Data from Qu [23], ♣ Data from Fujiwara [8], ♥ Data from Tajmir-Riahi [9].

3.2 THz-TDS Spectra of Chl-Mg-Na and Chl-*a*

Figure 4a shows the raw absorbance spectra for three pellets of Chl-Mg-Na (pellets 8-10) and one pellet of PE (pellet 18). The weak oscillations at low frequencies for the Chl-Mg-Na pellets are artefacts caused by multiple reflections of the probe beam through the sample, while well-resolved and sharp spectral features are observed above 1.3 THz. In addition, the observed background absorption may indicate the presence of amorphous regions in the Chl-Mg-Na samples. Due to the lack of long-range symmetry, all sharp spectral features disappear but absorption remains significant due to the random orientation of intermolecular bonds and scattering losses. The background corrected spectra obtained using the Vancouver algorithm with a 5^{th} order polynomial fit method for the four pellets are shown in Fig. 4b. For a clearer representation the data have been offset vertically. For the higher Chl-Mg-Na quantity (pellets 8 and 9), three well-resolved features were obtained at 1.44, 1.64, and 1.83 THz (Fig. 4b). An enlarged view of the features observed for Chl-Mg-Na above 1.3 THz is shown in Fig. 4c, and for comparison, the THz-TDS spectra of Chl-*a* was displayed in the inset of Fig. 2a. While some similarities with the Chl-*a* THz spectrum are observed, the strong features observed in Chl-*a* around 1.45 THz, 1.73 THz and 1.86 THz are slightly shifted towards lower frequencies for Chl-Mg-Na (0.01 THz, 0.09 THz and 0.03 THz, respectively). For the two polycrystalline species, these spectral features, as in many molecular crystals, may be explained as originating from mixed intermolecular and intramolecular vibrational modes. The differences between these spectral signatures highlight how different the long-range forces are in these two crystals. For the pellets with a

high quantity of Chl-Mg-Na, the feature around 1.96 THz was difficult to identify, as a direct consequence of limited dynamic range of the experiment, the sample signal reached the noise floor level of the experiment.

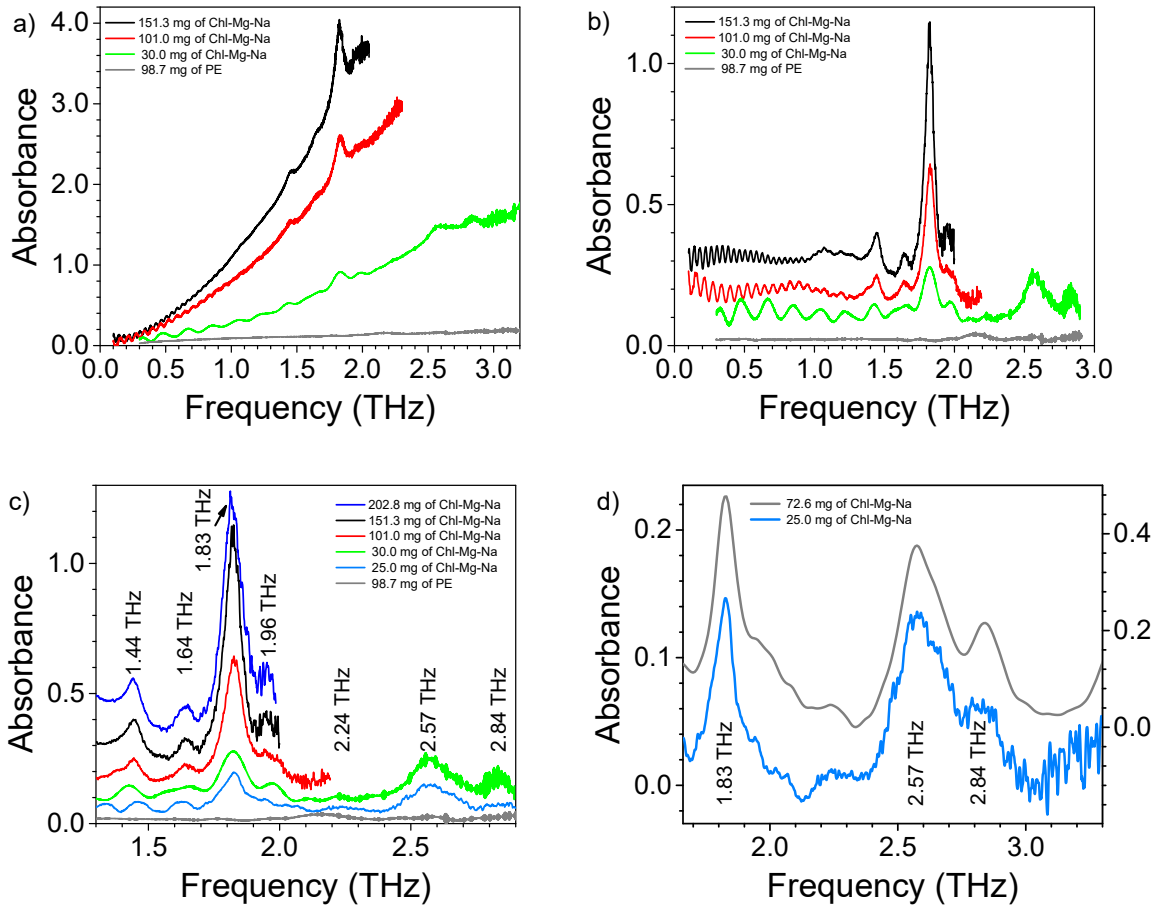

Fig. 4 a) Raw THz-TDS absorbance data for Chl-Mg-Na-PE pellets (pellet 8, black; pellet 9, red; pellet 10, green) and a PE pellet (pellet 18, grey). b) Corresponding background corrected absorbance. The different spectra are vertically offset for clarity. c) Enlarged view of the features above 1.3 THz for a pure Chl-Mg-Na sample (pellet 2, blue), Chl-Mg-Na-PE pellets (pellet 8, black; pellet 9, red; pellet 10, green; pellet 12, light blue), and a PE pellet (pellet 18, grey). d): A comparison of absorbance spectra for THz-TDS experiment (pellet 12, light blue, left axis) and FTIR experiment (pellet 5, grey, right axis).

To acquire robust absorption spectra above 1.9 THz, smaller amounts of Chl-Mg-Na were therefore required. The absorption features at low frequencies (pellets 10 and 12) significantly decrease in intensity, but the sample signal reached the noise floor level of the experiment at higher frequencies [13]. Thus, the features at 1.96, 2.24, 2.57 and 2.84 THz can be clearly observed. In addition, Fig. 4d shows that THz-TDS spectra and FTIR spectra are in good agreement, and demonstrate the reproducibility and complementarity of both techniques in this study. It was aforementioned that the Chl-Mg-Na powder includes a small percentage of magnesium stearate (< 0.5 wt-%) for lubricating purposes. In order to determine the effects magnesium stearate can have on the current study, pellets 19 and 20 were prepared with 0.5 and 2 wt-% of magnesium stearate in PE respectively (Table 1). As expected, no absorption peaks were observed in the THz frequency range (Fig. S3 provided in the Supporting Information), due to either the low concentration or to the amorphous nature of the magnesium stearate.

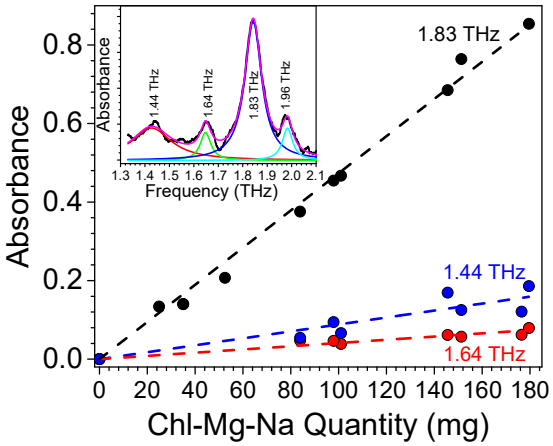

Fig. 5 Plot of the absorbance (after background subtraction) as a function of quantity of chlorophyll in the pellets at three frequencies (1.44, 1.64, and 1.83 THz). Inset: the frequency positions of the features were determined by a multipeak-fit using Lorentzian function (pellet 11).

The relatively strong and well-resolved features observed for Chl-Mg-Na samples present an opportunity for quantitative analysis. Therefore, we have investigated the response of the stronger features (1.44, 1.64, and 1.83 THz) with change of Chl-Mg-Na quantity. The frequency positions of the three peaks were determined by a multipeak-fit using Lorentzian function (Inset of Fig.5) with amplitude, full-width half-maxima, and offset set as parameters. Figure 5 presents the plot of the absorbance (after background subtraction) as a function of quantity of Chl-Mg-Na in the pellet. This was done at all three frequencies with a fitted line crossing zero referring to zero amount. As anticipated, the background corrected absorbance increases linearly with Chl-Mg-Na quantity in the pellet. The results clearly suggest that the feature at 1.83 THz can be used for quantification of chlorophyll in polycrystalline form.

3.3 Refractive Index and Absorption Coefficient of Chl-Mg-Na material extracted from THz-TDS data

THz-TDS is a powerful tool for unambiguously extracting precise and reliable intrinsic optical parameters from a wide range of samples with applications ranging from materials science to biology. Recently, the THz-TDS technique has been shown to be well suited to recover the multilayer opto-geometric organization of a leaf (200 to 500 µm thick). For example, an 8-layer structure has been revealed for a sunflower leaf,, with the detail of thicknesses and complex refraction indices [32]. Relying on these successful results, the technique was applied to investigate the temporal dehydration process of a sunflower leaf [33]. Leaf optical models in the visible and near-infrared wavelength domains have so far combined, among other things, the absorption coefficients of photosynthetic pigments, to determine an average refractive index of the leaf interior [34]. In these models, the refractive index of the biochemical constituents has been assumed to be independent of the wavelength, leading to inaccuracies in the simulated leaf transmittance and reflectance of the leaf. The refractive index values of the biochemical constituents, except those of water, are poorly known, especially in the THz frequency range. In some cases, the refractive index values of chlorophyll were required and had to be modeled by a Lorentz model [35]. Here, THz-TDS measurements can be used to measure this valuable index refractive index for the Chl-Mg-Na derivative at THz frequencies. To extract these parameters from the Chl-Mg-Na material (Supporting Information), we made use of the open-source time-fitting software called Fit@TDS and developed by Peretti *et al.* [36]. The software enables a user to compare the recorded temporal pulse with the modelled one using an optimization approach. We performed the THz-TDS measurements in a timing window of 500 ps with steps of 20 fs for optimal frequency resolution. In order to adequately fit the data and retrieve the refractive index, the absorption coefficient, the frequency, the width and the oscillator strength of the features observed in the THz range, we followed the methodology used in Ref. 36. First, the Fabry-Pérot oscillations were retrieved by fitting the transmission data of a pure Chl-Mg-Na pellet (pellet 6) using the simplest model. The resulting residual error obtained for each pellet exhibited broad, high frequency losses, hence we added the strong oscillator observed around 5.5 THz in the far-infrared measurements (Fig. 2b). To take into account the well-marked features in the absorption spectrum, we added the four oscillators associated with the features at 1.44, 1.64, 1.83, and 1.96 THz (Table 3). The experimental time-trace of the pellet recording in the time-domain and the resulting fitted time-trace are illustrated in Fig. 6a. The corresponding spectra in the frequency-domain are displayed in Fig. 6b. The fitted values of the real part of the refractive index $\boldsymbol{n(\omega)}$ and of the absorption coefficient $\alpha(\boldsymbol{\omega})$ are shown in Figs. 6c and 6d, respectively. All absorption peaks are accompanied by a significant change in the refractive index near the feature. Below 1.0 THz, the Chl-Mg-Na material has a constant refractive index $\boldsymbol{n(\omega)}$ of approximately 2.09. The absorption coefficient

$\alpha(\omega)$ remains < 150 cm^{-1} below 2.5 THz. Table 3 lists the resulting fit parameters of the features, extracted from the pure Chl-Mg-Na pellet. It should be noted that the thickness extracted from the fit in the time-domain (408 µm), is in good agreement with the digital micrometer measurement (426 µm).

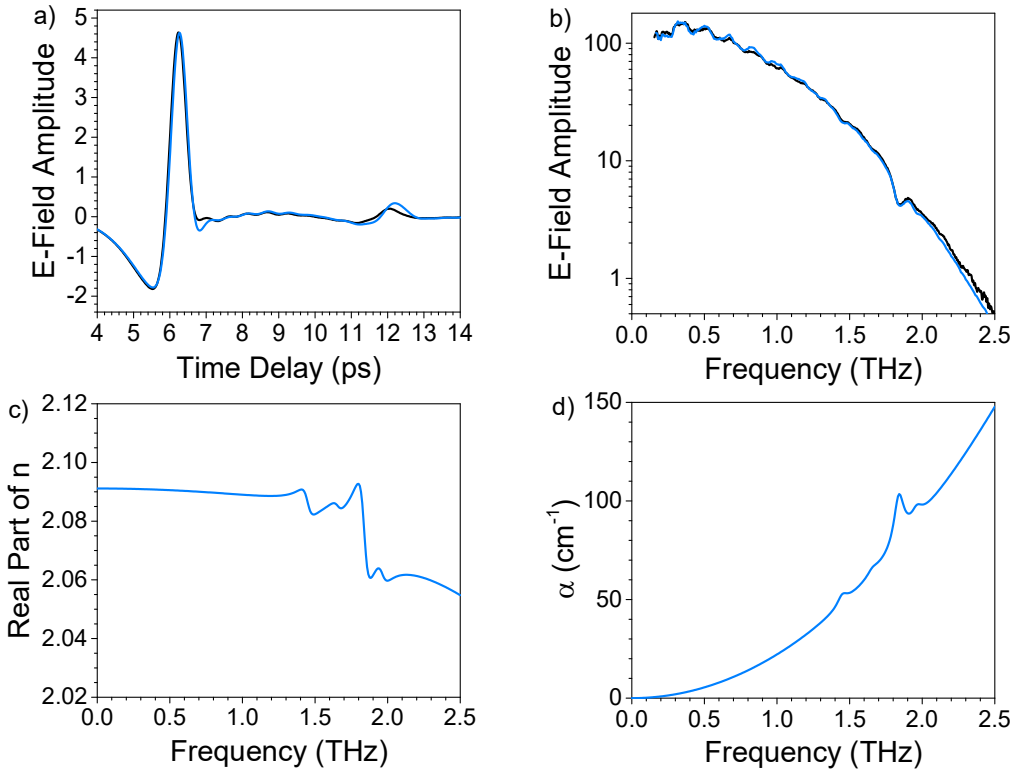

Fig. 6. a) Time-trace of the experimental data (black curve) obtained for a pure pellet of Chl-Mg-Na (pellet 6 with 77.8 mg of Chl-Mg-Na), compared with the results calculated using the FIT@TDS software [36] and the optimized parameters including the thickness, $n(\omega)$, $\alpha(\omega)$, and the 5 oscillators listed in Table 3 (light blue curve). b) Corresponding frequency-domain spectra. c) Fitted real part of the refractive index $n(\omega)$ and d) fitted absorption coefficient $\alpha(\omega)$.

Table 3 Optimized parameters for the first four absorption features of the 77.8-mg pure Chl-Mg-Na sample (pellet 6).

Fitted thickness: 408 µm, Permittivity at very high frequency: 3.833			
Oscillator	Oscillator Frequency [THz]	Oscillator Linewidth [THz]	Oscillator strength
1	1.449	84.3 10^{-3}	1.79 10^{-3}
2	1.659	85.3 10^{-3}	0.50 10^{-3}
3	1.836	87.9 10^{-3}	7.04 10^{-3}
4	1.963	81.2 10^{-3}	1.50 10^{-3}

3.4 Temperature dependence of the low frequency vibrational features for Chl-Mg-Na

Observing the temperature dependence of the low-frequency vibrational modes provides additional information and can play a decisive role in the assignment of the features. At 0 K, the motions of atoms around the equilibrium minima are well described by a harmonic potential. As temperature increases, a comparison of the experimental and calculated vibrational frequencies for most of the molecular crystals indicates the presence of pronounced anharmonicity in the intermolecular interactions [15,16]. In addition to anharmonicity, temperature-dependent structural changes can also have a large effect on vibrational features. Thus, as the temperature is increased, the

THz features experience notable line shape broadening and shifts in frequencies. Investigating the temperature changes of the low-frequency vibrational modes of chlorophyll is critical for future simulations and assignments of the modes at room temperature. Figure 7a shows the background corrected absorbance spectra of a pure Chl-Mg-Na pellet from 88 K to 298 K (pellet 7). The low-temperature spectra have significantly sharper, well-defined features.

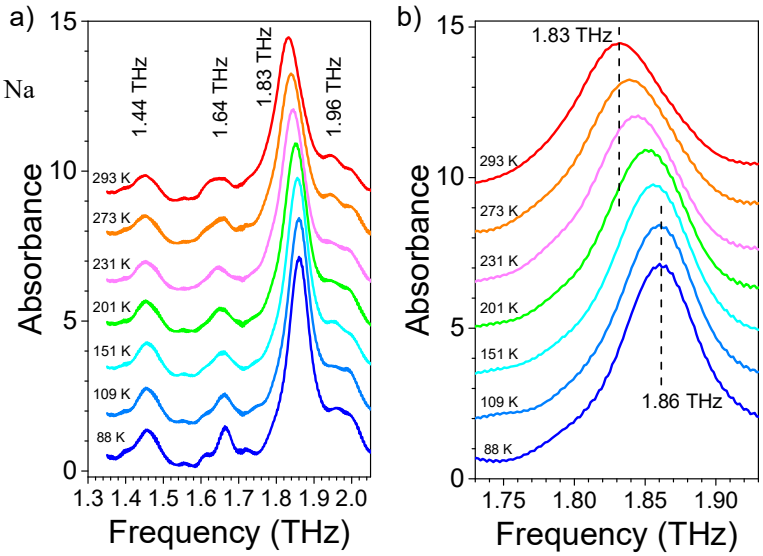

Fig. 7 a) Background corrected absorbance spectra of a pure Chl-Mg-sample (pellet 7 with 60.0 mg of Chl-Mg-Na) at temperatures from 88 K to 298 K. The different spectra are vertically offset for clarity. b) Enlarged view of the feature at 1.83 THz.

This thermal effect is particularly pronounced for the peak centred at 1.83 THz (Fig. 7b). The amplitude, frequency position, and full-width half-maxima of the four well-resolved features at 1.44, 1.64, 1.83, and 1.96 THz were determined by a multipeak fit using a Lorentzian function and these parameters were plotted against temperature in Figs. 8a, 8b, and 8c, respectively. As the temperature is increased (ΔT = 212 K), the changes in amplitude of the strong absorption peak centred at 1.83 THz is of 17%. Its red shift is pronounced with a value of 0.030 THz (1.0 cm^{-1}), while the changes in full-width half-maxima is of 0.02 THz (0.50 cm^{-1}). It should be noted that the effect would have been more marked when using THz spectra recorded at the lowest possible temperature to reduce the anharmonic effects. Interestingly, the spectral feature at 1.44 THz does not shift significantly and does not display a large temperature dependence in terms of amplitude and full-width half-maxima. This implies that anharmonicity and thermally induced structural changes only have a weak contribution in the cases of this vibrational mode. Further work to study the behaviour of the vibrational modes of Chl-Mg-Na without studying the temperature dependence has been done. This was carried out by introducing a small amount of solvent to the material to change the molecular environment and alter the intermolecular vibrational modes [37]. In a previous paper [38], we observed the changes of the THz features of Chl-Mg-Na pellets by changing the degree of hydration. The small amount of water in the Chl-Mg-Na polycrystals was easily removed under vacuum and as a consequence, as the sample dried the intensity of the 1.83 THz feature decreased and its position shifted to lower frequencies. After 6 h of dehydration, the 1.83 THz feature shifted by 0.014 THz (0.47 cm^{-1}) towards lower frequencies. In contrast, no drastic change was observed for the 1.44 THz feature. Additional experimental details are provided in the Supporting Information. The results are consistent with the temperature dependence, suggesting that the stronger feature at 1.83 THz is dominated by intermolecular vibrations in the Chl-Mg-Na polycrystals.

From this data, we have established THz spectral fingerprints for two chlorophyll species in polycrystalline form, Chl-*a* and Chl-Mg-Na, both of which contain a magnesium porphyrin complex in their molecular structure. These results offer the capability to aid in the identification and potential quantification of natural chlorophyll in plant tissues, an application that would be of particular value to the agronomy.

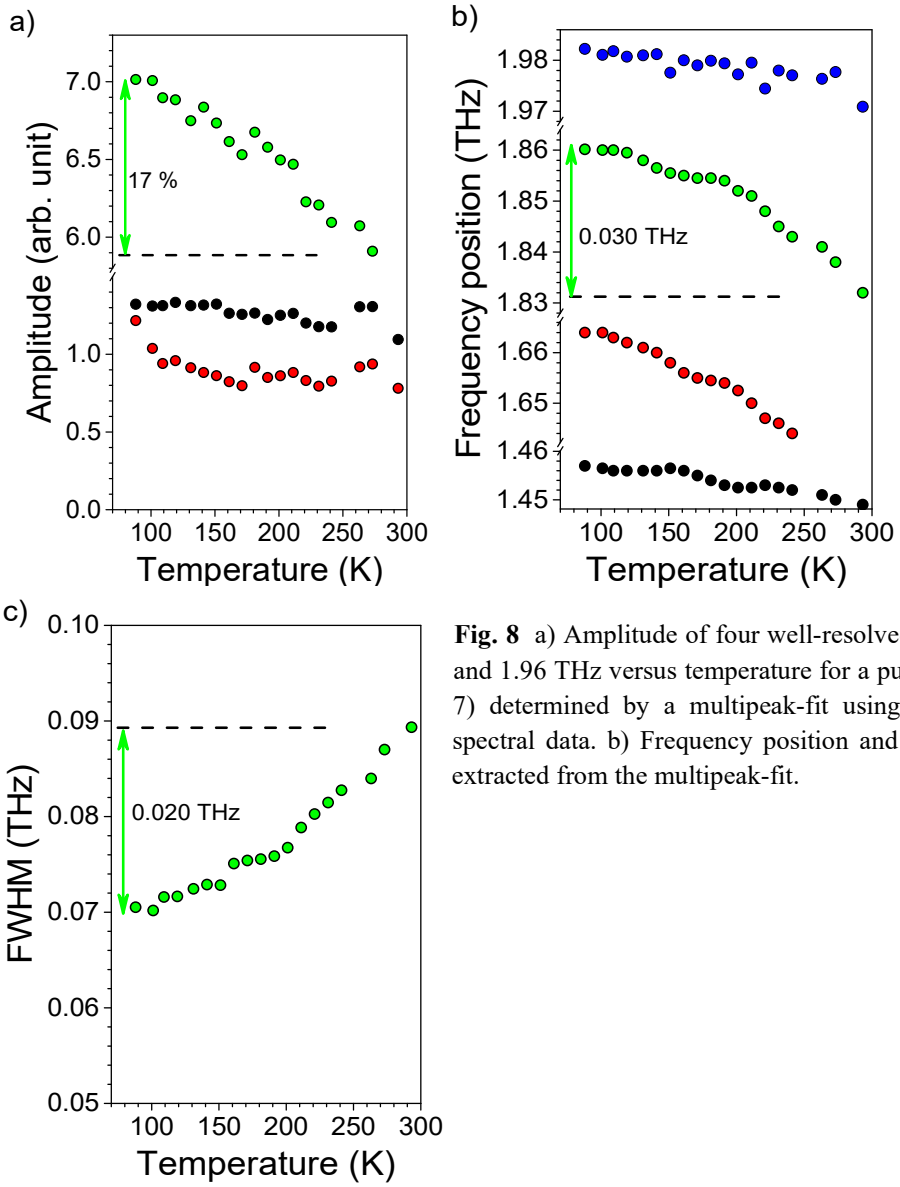

Fig. 8 a) Amplitude of four well-resolved features at 1.44, 1.64, 1.83, and 1.96 THz versus temperature for a pure Chl-Mg-Na sample (pellet 7) determined by a multipeak-fit using Lorentzian function of the spectral data. b) Frequency position and c) full-width half-maximum extracted from the multipeak-fit.

3.5 THz-TDS Spectra of chlorophyll in plant leaves

After the identification of the fingerprint of chlorophyll in polycrystalline form, our study focused on the detection of natural chlorophyll directly in plant tissues and in particular, in leaves. Estimating the concentration of leaf pigments using spectroscopy techniques has always been one of the most significant issues in plant sciences [39]. However, the overriding question concerning our study is: can we detect the presence of chlorophyll directly in a plant organ using THz spectroscopy? To address this issue, we have chosen to compare the THz absorption between green and non-green tissues of the leaves in variegated plants. Green sectors of pigment-related variegated plants contain high quantities of chlorophyll, while non-green sectors have little or no chlorophyll [40-42]. Here, leaves of variegated ivy shown in the inset of Fig. 9a were investigated. THz absorption spectra from pellets of dehydrated yellow and green tissues were measured. The first step of the experiments consisted to press dehydrated green and yellow tissues into pellets (20 and 21, respectively). This allowed to measure the chlorophyll absorption over a thickness greater than the thickness of a leaf and the formation of uniform, planar interfaces. THz-TDS measurements were performed at 298 K and 88 K (Fig. 9). The 298 K spectrum of the green pellet contains a very broad feature with a central frequency of 1.86 THz (62.0 cm^{-1}) (Fig. 9a), while the 88 K spectrum shown in the same figure has a significantly sharper peak that is more well-defined and with a central frequency of 1.87 THz (62.4 cm^{-1}). The frequency value obtained at 298 K remains very close to the one observed in our previous studies with isolated Chl-a. The yellow pellet showed a very weak feature at low

temperature with a central frequency of 1.86 THz (Fig. 9b). This indicates that the chlorophyll content in the yellow sectors of a variegated variety is low [40,41]. It should be noted that plants also contain Chl-*b* that can contribute to the diversity of recorded spectra. Thus, for a more comprehensive analysis, the investigation of low-frequency vibrations in Chl-*b* would be important for future studies. In the work presented herein, the low-frequency vibration around 1.86 THz suggests that long-range forces between chlorophyll molecules can form during the dehydration process. The self-aggregation (and crystal packing) is dense enough to show well-marked intermolecular vibrational modes.

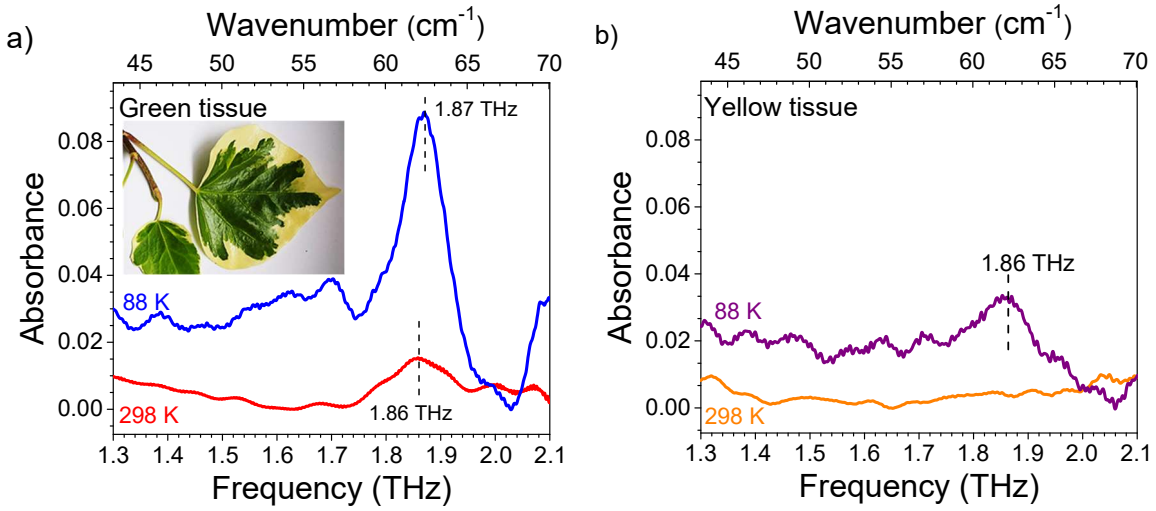

Fig. 9 THz-TDS background corrected absorbance spectra a) of dehydrated green ivy tissues pressed into pellet (pellet 20, with 100 mg of dehydrated green tissues) at 298 K (red) and 88 K (blue), and b) of dehydrated yellow ivy tissues pressed into pellet (pellet 21, with 92.5 mg of dehydrated yellow tissues) at 298 K (orange) and 88 K (violet). Inset: Leaf of the variegated ivy (*Aureomarginata* variety), showing a green centre, and a yellow margin and used for THz-TDS measurements.

Conclusions

In this paper, THz-TDS was used to measure the absorption properties of two chlorophyll polycrystalline powders: Chl-*a* and Chl-Mg-Na. The THz-TDS data of Chl- *a* agreed with previous reported studies, where sharp features were observed at 1.45, 1.73, and 1.86 THz. Previously unexplored Chl-Mg-Na material showed features which were slightly shifted compared to Chl- *a,* at 1.44, 1.64, 1.83, 2.57, and 2.84 THz. The temperature-dependent THz absorption spectra for Chl-Mg-Na provided additional information that will play a decisive role in the future assignment of the features. The temperature dependence reveals the presence of pronounced anharmonicity for the 1.83 THz feature and suggests that this feature is dominated by intermolecular vibrational modes. However, it is crucial that simulation methods are performed to facilitate the interpretation of experimental results shown here, and identify the vibrational motions in the molecular crystal structures. Our work with polycrystalline powders of Chl-*a* and ChI-Mg-Na allowed us to obtain an optimised enough measurement process to detect chlorophyll directly in plant tissues. Using dehydrated leaves of a common variegated ivy plant (*Aureomarginata* variety), a clear absorption feature was observed at 1.87 THz at 88 K. By studying different sectors of the plant leave, we were able to show trends between the intensity of the fingerprint region features and the concentration of chlorophyll, where green sectors gave more intense peaks compared with yellow sectors.

These findings are very promising as first steps towards detection and quantification of chlorophyll in plants using THz-TDS. Pursuing and developing this work will add new entries to the ever-growing list of applications for THz in the agro-environmental field, a field which is becoming increasing important for the future of sustainability on our planet.

Acknowledgements

This project was supported by the Montpellier University of Excellence I-Site MUSE (PRIME@MUSE), by the Contrat de Plan Etat-Région (CPER) - Région Occitanie “PlantEnvi”, and has received funding from the European Union’s Horizon 2020 research and innovation programme under grant agreement N° 964203 (FET-Open LINkS project).The authors thank Catalyons Laboratories for providing chlorophyll derivative powders.

Ethical Approval

The work and the drafting of this paper follow the ethical and professional principles of the authors and other external people involved. The research does not involve human participants.

Consent to Participate

No external participation is foreseen for this work.

Consent to Publish

If the research is accepted for publication, I consent to publish this work in the *Journal of Infrared, Millimeter, and Terahertz Waves*.

Authors Contributions

D.C. and N.D. conceived the idea and secured funding for this research. All authors designed the experiments. Y.M. prepared some of the samples. D.C., N.D., E.O., E.B. performed all of the experiments and measurements. D.C., N.D., E.O., E.B., and C.B. performed analysis. All authors interpreted the results. D.C., E.O., and E.B. wrote the main manuscript and prepared the figures. The manuscript was written through contributions of all authors: D.C., E.O., E.B., Y.M., C.B., D.N., K.F., J.T., N.D.. All authors reviewed the manuscript.

Funding

The Montpellier University of Excellence I-Site MUSE (PRIME@MUSE),
The Contrat de Plan Etat-Région (CPER) - Région Occitanie "PlantEnvi"
Funding from the European Union's Horizon 2020 research and innovation programme under grant agreement N° 964203 (FET-Open LINkS project)

Competing Interests

The authors have no competing interests.

Availability of data and materials

The datasets generated for this study are available from the corresponding authors on reasonable request.

ORCID iD
Dominique Coquillat − https://orcid.org/0000-0002-0574-7010
Etienne V. Brouillet − https://orcid.org/0000-0002-4120-2384
Cédric Bray − https://orcid.org/0000-0002-6813-0931
David J. Nelson https://orcid.org/0000-0002-9461-5182
Karen Faulds − https://orcid.org/0000-0002-5567-7399
Jeremie Torres − https://orcid.org/0000-0001-5874-0990
Nina Dyakonova − https://orcid.org/0000-0002-4365-4974

References

1. B. Gajewska, S. Raccio, K. J. Rodriguez and N. Bruns, *Polymer Chemistry*, 10, 125−135 (2019), https://doi.org/10.1039/C8PY01492B
2. S. Y. Chen, Y. Y. Lu, F. Y. Shih, P. Ho, Y. F. Chen, C. Chen, Y. T. Chen and W. H. Wang, *Carbon*, 63, 23-29 (2013), https://doi.org/10.1016/j.carbon.2013.06.031
3. Y. Yu, Y. Zhang, L. Jin, Z. Chen, Y. Li, Q. Li, M. Cao, Y. Che, H. Dai, J. Yang and J. Yao, *Org. Electron.*, 65, 381–385 (2019), https://doi.org/10.1016/j.orgel.2018.11.039
4. B. Yang, Y. Lu, D. H. Jiang, Z. C. Li, Y. Zeng, S. Zhang, Y. Ye, Z. Liu, Q. Q. Ou, Y. Wang, S. L. Dai, Y. P. Yi and J. Huang, *Adv. Mater.*, 32, 2001227 (2020), https://doi.org/10.1002/adma.202001227
5. S. Erten-Ela, K. Ocakoglu, A. Tarnowska, O. Vakuliuk and D. T Gryko, *Dyes and Pigments*, 114, 129-137 (2015), https://doi.org/10.1016/j.dyepig.2014.11.008
6. S. Duan, Q. Zhou, A. Li, X. Wang, S. Sasaki and H. Tamiaki, *Sol. RRL*, 4: 2000162 (2020), https://doi.org/10.1002/solr.202000162
7. L. J. Boucher, H. H. Strain and J. J Katz, *J. Am. Chem. Soc.*, 88, 7, 1341–1346 (1966), https://doi.org/10.1021/ja00959a001

8. M. Fujiwara, H. Hayashi and M. Tasumi, *Croatica Chemica Acta*, 61, 435-446 (1988), https://doi.org/10.1002/chin.198906046
9. H. A. Tajmir-Riahi, G. Wang and R. M. Leblanc, *Photochemistry and Photobiology*, 54, 265-271 (1991), https://doi.org/10.1111/j.1751-1097.1991.tb02015.x
10. L. L. Thomas, J. H. Kim and T. M. Cotton, *J. Am. Chem. Soc.*, 112, 25, 9378–9386 (1990), https://doi.org/10.1021/ja00181a046
11. C. Zhou, J. R. Diers and D. F. Bocian, *J. Phys. Chem. B*, 101, 9635-9644 (1997), https://doi.org/10.1021/jp971965g
12. J. A. Zeitler, P. F. Taday, D. A. Newnham, M. Pepper, K. C. Gordon and T. Rades, *J. Pharm. Pharmacol.*, 59, 209-23 (2007), https://doi.org/10.1211/jpp.59.2.0008
13. P. Jepsen, D. Cooke and M. Koch, *Laser Photonics Rev.*, 5: 124-166 (2011), https://doi.org/10.1002/lpor.201000011
14. F. Zhang, H.-W. Wang, K. Tominaga and M. Hayashi, *J. Phys. Chem. A*, 119, 3008−3022 (2015), https://doi.org/10.1021/jp512164y
15. M. T. Ruggiero and J. A. Zeitler, *J. Phys. Chem. B*, 120, 11733–11739 (2016), https://doi.org/10.1021/acs.jpcb.6b10248
16. M. T. Ruggiero, J. A. Zeitler and A. Erba, *Chem. Commun.*, 53, 3781-3784 (2017), https://doi.org/10.1039/C7CC00509A
17. J. Neu, H. Nikonow and C. A. Schmuttenmaer, *J. Phys. Chem.* A, 122, 28, 5978-5982 (2018), https://doi.org/10.1021/acs.jpca.8b04978
18. P. Bawuah and J. A. Zeitler, *TrAC Trends Anal. Chem.*, 139, 116272 (2021), https://doi.org/10.1016/j.trac.2021.116272
19. K. Siegrist, C. R. Bucher, I. Mandelbaum, A. R. Hight Walker, R. Balu, S. K. Gregurick, and D. F. Plusquellic, *J. Am. Chem. Soc.*, 128, 5764-5775 (2006), https://doi.org/10.1021/ja058176u
20. D. Lee, H. Cheon, S. Jeong and J. Son, Sci Rep, 10, 10271 (2020), https://doi.org/10.1038/s41598-020-67179-z
21. M.O. Senge, A.A. Ryan , K.A. Letchford, S.A. MacGowan and T. Mielke, Chlorophylls, Symmetry, Chirality, and Photosynthesis. *Symmetry*, 6, 781-843 (2014).
22. H. Chen and L. Wang, *J. Appl. Phys.* 102, 074701 (2007), https://doi.org/10.1063/1.2787956
23. Y. Qu, H. Chen, X. Qin, L. Wang, L. Li and T. Kuang, *Sci China C Life Sci.*, 50, 350-355 (2007), https://doi.org/10.1007/s11427-011-4213-7
24. C. Wagner, C. Peveling-Oberhag, C. Heinen, F. Fritzsche, A. Hommes, D. Nüßler and H. Essen, *IEEE, 36th International Conference on Infrared, Millimeter, and Terahertz Waves, IRMMW-THz 2011*, Houston, Texas, USA (2011), https://doi.org/10.1109/irmmw-thz.2011.6104751
25. L. Jiang, J. Yu, C. Li, Y. Xu, B. Jin and Y. Liu, *IEEE, 40th International Conference on Infrared, Millimeter, and Terahertz Waves, IRMMW-THz 2015*, Hong Kong, China (2015), https://doi.org/10.1109/IRMMW-THz.2015.7327437
26. S. Matsubara and H. Tamiaki, *Applied Nano Materials*, 3, 1841-1847 (2020), https://doi.org/10.1021/acsanm.9b02510
27. Liu Yi-Ke, Liu Yu-Tong, Xu Xiang-Dong, Yan Wei, Ma Miao, Zhu Hong-Zhao, Ma Chun-Qian, Zou Rui-Jiao Ding Lian and Luo Meng-Jia, Acta Physica Sinica, 64, 068701, (2015), https://doi.org/10.7498/aps.64.068701
28. Y. L. Wang, Z. K. Zhou, X. N. Peng, L. Zhou, Z. H. Hao and Q. Q. Wang, *Chin. Phys. Lett.*, 30, 098702 (2013), https://doi.org/10.1088/0256-307X/30/9/098702
29. J. Zhao, H. Lui, D. I. McLean and H. Zeng, *Appl. Spectrosc.*, 61, 1225-32, (2007), https://doi.org/10.1366/000370207782597003
30. D. Graham, K. Faulds and W. E. Smith, *Chem. Commun.*, 4363-4371, (2006), https://doi.org/10.1039/B607904K
31. K. Faulds, R. E. Littleford, D. Graham, G. Dent and W. E. Smith, *Anal. Chem.*, 76, 592-598 (2004), https://doi.org/10.1021/ac035053o
32. Y. Abautret, D. Coquillat, M. Zerrad, X. Buet, R. Bendoula, G. Soriano, N. Brouilly, D. Héran, B. Grèzes-Besset, F. Chazallet and C. Amra, *Opt Express* 28, 35018-35037 (2020), https://doi.org/10.1364/OE.400852

33. Y. Abautret, D. Coquillat, M. Lequime, M. Zerrad and C. Amra, *Opt. Express* 30, 37971-37979 (2022), https://doi.org/10.1364/OE.400852
34. J.-B. Feret, C. François, G. Asner, A. Gitelson, R. Martin, L.P. Bidel, S. L. Ustin, G. le Maire, S. Jacquemoud, *Remote Sensing of Environment* 112, 3030–3043 (2008), https://doi.org/10.1016/j.rse.2008.02.012
35. S. Q. Achí and W. E. V. Castro, *Chromatogr Spectrosc Tech* 4, 48-60 (2021). https://doi.org/10.36959/326/772
36. R. Peretti, S. Mitryukovskiy, K. Froberger, M. Mebarki, S. Eliet, M. Vanwolleghem and J. F. Lampin, *IEEE Transactions on Terahertz Science and Technology*, 9, 136-149 (2019), https://doi.org/10.1109/TTHZ.2018.2889227
37. N. Nagai, R. Kumazawa and R. Fukasawa, *Chem. Phys. Lett.*, 413, 495-500 (2005), https://doi.org/10.1016/j.cplett.2005.08.023
38. D. Coquillat, E. O'Connor, E. V. Brouillet, Y. Meriguet, C. Bray, D. J. Nelson, K. Faulds, J. Torres and N. Dyakonova, *Proc. SPIE* 2021, 11827, *Terahertz Emitters, Receivers, and Applications XII*, 118270F (2021), https://doi.org/10.1117/12.2593589
39. J. B. Féret, A. A. Gitelson, S. D. Noble and S. Jacquemoud, *Remote Sensing of Environment*, 193, 204-215 (2017), https://doi.org/10.1016/j.rse.2017.03.004
40. G. Manenti and G. Tedesco, *Caryologia*, 30, 163-176 (1977), https://doi.org/10.1080/00087114.1977.10796689
41. S. H. Pao, J. W. Liu, J. Y. Yang, P. Chesson and C. R. Sheue, *Taiwania*, 65, 74-80 (2020), https://doi.org/10.6165/tai.2020.65.74
42. Q. Zhang, J. Huang, P. Zhou, M. Hao and M. Zhang, *Plants*, 10, 552 (2021), https://doi.org/10.3390/plants10030552